



Hemodynamic assessments of unilateral pulsatile tinnitus with jugular bulb wall dehiscence using 4D flow magnetic resonance imaging

Chihang Dai^{1^}, Pengfei Zhao^{1#^}, Guopeng Wang^{2#^}, Heyu Ding^{1^}, Han Lv¹, Xiaoyu Qiu^{1^}, Ruowei Tang^{1^}, Ning Xu^{1^}, Yan Huang^{1^}, Kaixuan He², Zhenghan Yang^{1^}, Shusheng Gong^{2^}, Zhenchang Wang^{1#^}

¹Department of Radiology, Beijing Friendship Hospital, Capital Medical University, Beijing, China; ²Department of Otolaryngology Head and Neck Surgery, Beijing Friendship Hospital, Capital Medical University, Beijing, China

Contributions: (I) Conception and design: P Zhao, C Dai; (II) Administrative support: P Zhao, H Ding, H Lv, Z Wang; (III) Provision of study materials or patients: H Ding, Z Yang, S Gong; (IV) Collection and assembly of data: C Dai, K He, G Wang; (V) Data analysis and interpretation: C Dai, K He, R Tang, N Xu, Y Huang; (VI) Manuscript writing: All authors; (VII) Final approval of manuscript: All authors.

#These authors contributed equally to this work.

Correspondence to: Pengfei Zhao, MD, PhD. Department of Radiology, Beijing Friendship Hospital, Capital Medical University, 95 Yong'an Road, Xicheng, Beijing 100050, China. Email: zhaopengf05@163.com; Guopeng Wang, MD, PhD. Department of Otolaryngology Head and Neck Surgery, Beijing Friendship Hospital, Capital Medical University, 95 Yong'an Road, Xicheng, Beijing 100050, China. Email: guopengent@163.com; Zhenchang Wang, MD, PhD. Department of Radiology, Beijing Friendship Hospital, Capital Medical University, 95 Yong'an Road, Xicheng, Beijing 100050, China. Email: cjr.wzhch@vip.163.com.

Background: Pulsatile tinnitus (PT) is a type of tinnitus characterized by a rhythmic sound that is synchronous with the heartbeat. One of the possible causes of PT is the jugular bulb wall dehiscence (JBWD). However, the hemodynamics of this condition are not well understood. To elucidate this issue, the present study aimed to compare the blood flow of PT patients with JBWD, PT patients with sigmoid sinus wall dehiscence (SSWD), and volunteers.

Methods: A retrospective case-control study was conducted, which enrolled patients with unilateral PT who had undergone both computed tomography angiography (CTA) and four-dimensional (4D) flow magnetic resonance imaging (MRI) examinations at the Department of Otolaryngology-Head and Neck Surgery of Beijing Friendship Hospital affiliated to Capital Medical University between January 2019 and July 2023. After excluding the possible causes of PT, the patients were divided into the JBWD group and SSWD group according to the presence or absence of JBWD and/or SSWD. Finally, 11 female unilateral PT patients with JBWD (JBWD group, 11sides), 22 age- and side-matched female patients with SSWD (SSWD group, 22 sides), and 22 age-matched female volunteers (volunteer group, 36 sides) were enrolled. The area, maximum voxel velocity (V_{v-max}), maximum velocity (V_{max}), average velocity (V_{avg}), and average blood flow rate (Q) were measured in the transverse sinuses (TSs), sigmoid sinuses (SSs), and jugular bulb (JB). The vortex flow pattern was also assessed. Fisher's exact test and Bonferroni correction were used for count data, with $P < 0.017$ was considered statistically significant. Shapiro-Wilk test, one-way analysis of

^ ORCID: Chihang Dai, 0000-0002-0209-6742; Pengfei Zhao, 0000-0002-9210-6544; Guopeng Wang, 0000-0002-5947-3131; Heyu Ding, 0000-0003-1519-6141; Xiaoyu Qiu, 0000-0003-1888-2964; Ruowei Tang, 0000-0002-0747-6672; Ning Xu, 0000-0001-6330-873X; Yan Huang, 0009-0001-2298-3971; Zhenghan Yang, 0000-0002-8473-3257; Shusheng Gong, 0000-0001-6847-3195; Zhenchang Wang, 0000-0001-8190-6469.

variance (ANOVA), Kruskal-Wallis H test, paired-samples t -test, and Wilcoxon matched-pairs signed-rank test were used for continuous variables depending on the distribution and variance of the data. The $P < 0.05$ and corrected $P < 0.05$ was considered statistically significant.

Results: The area and Q of TSs and JB on the symptomatic side were higher than those on the contralateral side in the JBWD group (TSs: $P_{\text{area}}=0.004$, $P_{\text{flow}}=0.002$; JB: $P_{\text{area}}=0.034$, $P_{\text{flow}}=0.018$). The area was larger and velocities were lower in the JBWD group at the TSs than the SSWD group ($P_{\text{area}}=0.004$, $P_{V_{v-\text{max}}}=0.009$, $P_{V_{\text{max}}}=0.021$, $P_{V_{\text{avg}}}=0.026$), and velocities were higher at the distal TSs and SSs than the volunteer group (TSs: $P_{V_{v-\text{max}}}=0.042$, $P_{V_{\text{max}}}=0.046$, $P_{V_{\text{avg}}}=0.040$; SSs: $P_{V_{v-\text{max}}}=0.007$, $P_{V_{\text{max}}}=0.001$, $P_{V_{\text{avg}}}=0.001$). At the JB, the JBWD group also had higher $V_{v-\text{max}}$ than the volunteer group ($P=0.012$). The occurrence rate of vortex at JB in the JBWD group was higher than both the JBWD and the volunteer groups ($P=0.002 < 0.017$ and $P=0.009 < 0.017$, respectively).

Conclusions: The blood flow of the intracranial venous sinus was different between the JBWD group and the SSWD group. The indicators that can differentiate include $V_{v-\text{max}}$, V_{max} , V_{avg} , vortex, and TSs cross-sectional area.

Keywords: Pulsatile tinnitus (PT); jugular bulb (JB); transverse sinus (TS)

Submitted May 31, 2023. Accepted for publication Nov 10, 2023. Published online Jan 02, 2024.

doi: 10.21037/qims-23-781

View this article at: <https://dx.doi.org/10.21037/qims-23-781>

Introduction

Pulsatile tinnitus (PT), which is predominantly curable, is a form of tinnitus characterized by a rhythmic noise that follows the heartbeat without external stimuli and accounts for about 4% of all tinnitus (1,2). If PT persists over a long period, it can negatively affect mental and physical health and lead to functional and structural cerebral changes (3,4). Consequently, it is crucial to identify the underlying PT causes, and noninvasive imaging plays an important role in the diagnosis of PT (5). Causes can be detected in over 70% of patients through computed tomography (CT) (6).

PT is attributed to arterial and venous causes (7-9). Venous PT is the most common cause, accounting for up to 84% (7,10), and this group of patients can be distinguished from those with arterial PT by compressing the symptomatic jugular vein to reduce the tinnitus intensity (11). Based on CT examination, many studies have shown that the key factor in venous PT is the absence of bone wall dehiscence (12,13). Most cases of venous PT have been linked to sigmoid sinus wall dehiscence (SSWD) with or without diverticulum, making this the most studied and reported form of venous PT (7). Furthermore, jugular bulb wall dehiscence (JBWD) is another common imaging feature of PT patients, affecting about 13.6% (7), but it has received little attention.

A growing body of research demonstrates that blood

flow is the source of PT sounds, and that hemodynamics are involved in the development of wall anomalies (14-16). However, most previous investigations on hemodynamics in PT patients did not distinguish between the two venous PT types (14,17). Transverse sinus (TS) stenosis causes higher blood velocity and flow rate, which is critical to bone abnormalities in PT associated with SSWD (15,18). A recent paper presented differences in CT findings between PT patients with JBWD and SSWD, suggesting that the upstream vascular morphology of the jugular bulb (JB) differs between the two groups (19). However, the hemodynamic characteristics of PT with JBWD and the differences between the JBWD and SSWD groups remain poorly understood.

CT and magnetic resonance (MR) angiography (CTA and MRA, respectively) can show intracranial sinuses, but only yield anatomical information (1,20). Transcranial ultrasound can observe and measure the veins and blood flow with high resolution but depends on the bone window (21). Digital subtraction angiography (DSA) has high resolution and can detect blood flow direction and speed, but it is invasive and has high radiation and risks (22). Phase contrast (PC) MR imaging (MRI) enables the visualization and measurement of blood flow *in vivo*. This lays the groundwork for four-dimensional (4D) flow MRI, a diagnostic modality that does not require radiation or contrast agents (23). This

evolving technology is increasingly being used to assist in the diagnosis of intracranial diseases (14,24-27).

This work investigated the hemodynamics of the intracranial TS, sigmoid sinus (SS), and JB of all participants. The aim of this study was to assess the hemodynamic features of PT in patients with JBWD and compare them with those of patients with SSWD using 4D flow MRI, and to provide a hemodynamic basis for the clinical differentiation of the two types of PT. We present this article in accordance with the STROBE reporting checklist (available at <https://qims.amegroups.com/article/view/10.21037/qims-23-781/rc>).

Methods

This study was conducted in accordance with the Declaration of Helsinki (as revised in 2013). The study was approved by the Ethics Committee of Beijing Friendship Hospital Affiliated to Capital Medical University (Nos. 2020-P2-202-02 and 2023-P2-095-01), and informed consent was provided by all the patients.

From January 2019 to July 2023, a total of 1,972 consecutive patients came to the Department of Otolaryngology-Head and Neck Surgery of Beijing Friendship Hospital Affiliated to Capital Medical University due to experiencing PT. A total of 157 patients with unilateral PT had previously undergone both CT angiography and 4D flow MRI.

CTA images of 157 patients with unilateral PT were retrospectively analyzed, and the exclusion criteria for the experimental group were as follows: (I) arterial PT, which could not be eliminated or significantly alleviated by ipsilateral jugular compression; (II) PT suspected to be caused by metabolic causes; (III) arteriovenous abnormality (e.g., dural arteriovenous fistula); (IV) PT suspected to be caused by other potential small veins with surrounding bone wall dehiscence (e.g., mastoid emissary veins, diploic vein); (V) intracranial tumor (e.g., paraganglioma, endolymphatic sac tumor, meningioma, vascular metastases, hemangiopericytoma, hemangioma); (VI) patients without any suspected PT-related bone wall dehiscence; and (VII) patients with both SSWD and JBWD. After excluding other suspicious factors that could cause PT, patients were classified into two categories based on the presence of JBWD or SSWD on imaging: those with isolated SSWD without JBWD (90 patients) and those with isolated JBWD without SSWD (11 patients). All 11 unilateral PT patients (right/left, 8/3) with isolated JBWD without SSWD were

enrolled in the JBWD group (11 symptomatic sides); all were females with an average age of 40 ± 10 years old. Consecutive 22 age- and side-matched female patients with isolated SSWD and without JBWD were enrolled at a ratio of 1:2 (22 symptomatic sides, SSWD group, 37 ± 13 years). Furthermore, 22 age-matched female healthy controls (44 sides, volunteer group, 38 ± 14 years) were enrolled at a ratio of 1:2. The specific inclusion and exclusion processes of the JBWD and the SSWD groups are shown in *Figure 1*.

Imaging technique

CTA was performed using a Brilliance 64-slice CT scanner (Philips Healthcare, Best, The Netherlands) with a bolus tracking program (Trigger Bolus software; Philips Healthcare). All patients were placed in the supine position. The parameters were the same as those reported in European Radiology (1).

4D flow MRI data were derived from 3.0 T MRI (Ingenia; Philips Healthcare) with a 32-channel standard head coil. The velocity encoding (VENC) of 4D flow MRI was flexibly evaluated from two-dimensional (2D) PC MRI results. The acquisition plane of 2D PC MRI was perpendicularly positioned at the distal end of the stenosis or the distal TS of the symptomatic side. The VENC for 2D PC MRI was first set to 40 cm/s; if velocity aliasing emerged in the image, the VENC value was increased in 20 cm/s increments until the aliasing was eliminated (28). Then, this final VENC of 2D PC MRI was set as the VENC of 4D flow MRI. The acquisition parameters of 2D PC MRI and 4D flow MRI are shown in *Table 1*.

Blood flow visualization and measurement

4D flow MRI images were processed by GTFlow (version 2.2.15; Gyro Tools, Zurich, Switzerland). The data were preprocessed before visualization and quantification, which included applying velocity masks, correcting velocity aliasing and eddy currents. Velocity masks were created using intensity-based masks and velocity threshold masks from 10 to 150 cm/s. Phase aliasing was manually corrected voxel-by-voxel in all three flow directions. The linear phase offsets caused by eddy currents were usually corrected automatically.

On the magnitude image, the target vessel needs to be manually drawn with cross-section lines to measure the hemodynamic parameters, and all the measurement planes are perpendicular to the vessel. A total of three

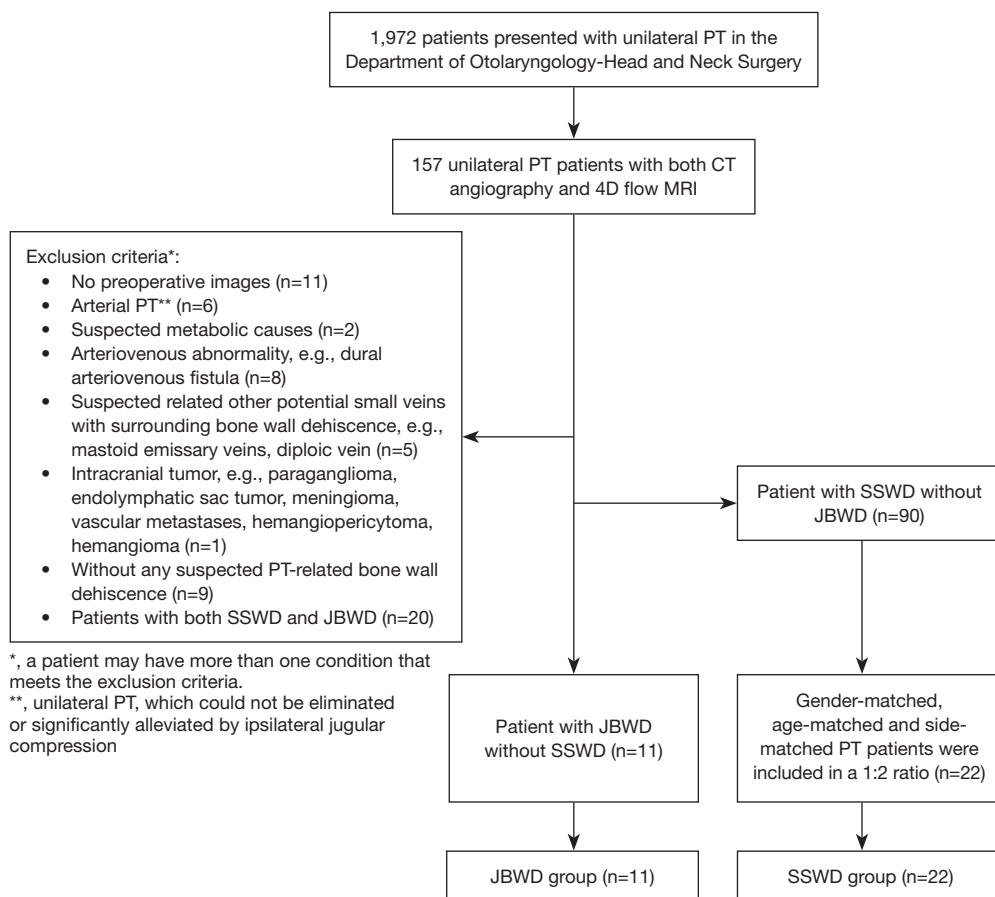


Figure 1 Flow chart of the inclusion and exclusion processes of the JBWD group and the SSWD group in PT patients. PT, pulsatile tinnitus; CT, computed tomography; 4D, four-dimensional; MRI, magnetic resonance imaging; SSWD, sigmoid sinus wall dehiscence; JBWD, jugular bulb wall dehiscence.

Table 1 Acquisition parameters of 2D PC MRI and 4D flow MRI

Parameters	2D PC MRI	4D flow MRI
TR (ms)/TE (ms)	10/5.8	7.2/3.3
Flip angle (°)	10	20
Acquired voxel size (mm ² /mm ³)	1×1	1×1×1
Field of view (mm ² /mm ³)	161×161	161×161×40
Matrix size (mm ² /mm ³)	160×162	160×160×40
Bandwidth (Hz/pixel)	192	193
Reconstructed voxel size (mm ² /mm ³)	0.31×0.31	0.46×0.46×1
Cardiac phases	–	16
Scan time (min)	1.5	6

2D, two-dimensional; PC, phase contrast; MRI, magnetic resonance imaging; 4D, four-dimensional; TR, repetition time; TE, echo time.

planes were measured: the distal TS, the middle SS, and the lower boundary of the JB. PT patients in the JBWD group and healthy volunteers were evaluated for bilateral sinuses. PT patients in the SSWD group were evaluated for symptomatic sinuses, and the contralateral asymptomatic sinuses of this group were not included.

MR venography was used to measure the sinus cross-section area. As for quantification of blood flow (Figure 2), maximum voxel velocity (V_{v-max} , cm/s) and maximum velocity (V_{max} , cm/s) that passes through vessel cross sections were implemented at the time when peak velocity appears. V_{v-max} was defined as the highest velocity of all the voxels passing through the vessel cross-section in a cardiac cycle. V_{max} was defined as the peak value at which the average velocity (V_{avg} , cm/s) of all the voxels in the vessel cross-section over a cardiac cycle. The V_{avg} was the average

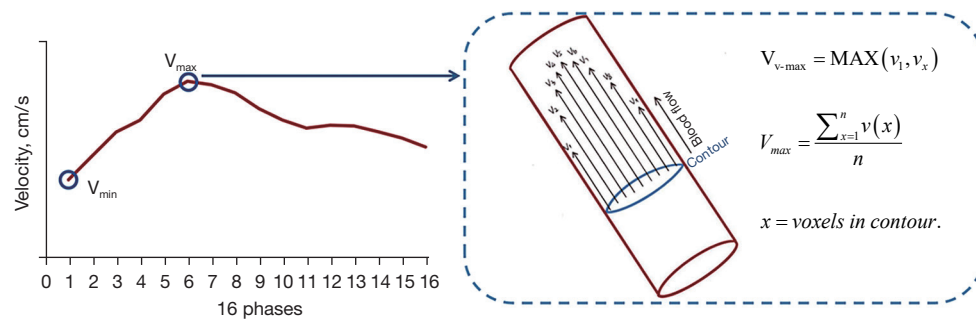


Figure 2 A diagram of velocities within a vessel cross section. Velocity values were named from V_1 to V_x , where x is the number of voxels in the plane. V_{v-max} (cm/s) was the highest velocity of all the voxels passing through the vessel cross section in a cardiac cycle. V_{max} and V_{min} (cm/s) were the peak and the lowest value of all the voxels in the vessel cross section over a cardiac cycle, respectively. V_{v-max} , maximum voxel velocity; V_{max} , maximum velocity; V_{min} , minimum velocity.

of all 16 velocities within a cardiac period. The average blood flow rate (Q , mL/s) was the mean flow rate value of all 16 phases passing through vessel cross-sections within a cardiac period. The area, velocity, and Q were evaluated independently by two neuroradiologists with 5 and 8 years of experience. The two radiologists were blinded to the patient's clinical information.

Flow patterns were assessed by two neuroradiologists independently, and disagreements were settled by consensus. The vortex flow pattern had a streamlined form defined as a ring-shaped spin loop.

Statistical analysis

Statistical analysis was performed using SPSS 22.0 software (IBM Corp., Armonk, NY, USA). For the count data, Fisher's exact test (the expected frequency was less than 5) was performed to test the association between the dependent variable and the independent variable. Then, pairwise comparisons were conducted using the Bonferroni correction method. Since there were three groups in this study, $P < 0.017$ (two-sided test) indicated a statistically significant difference.

The Shapiro-Wilk test was used to test the deviation of the data from the normal distribution. If the P value was greater than 0.05, we assumed that the data followed a normal distribution. Continuous variables with normal distribution were expressed as mean \pm standard deviation, and continuous variables with non-normal distribution were expressed as median [interquartile range (IQR)]. For the

comparison of measured values among the three groups (JBWD group, SSWD group, and volunteer group), one-way analysis of variance (ANOVA) was used if the data met the assumptions of normality and homogeneity of variance, otherwise Kruskal-Wallis H test was used, followed by *post-hoc* analysis (Bonferroni correction) to determine the specific differences among them. For the comparison of bilateral venous blood flow parameters in the same patient in the JBWD group, paired-samples t -test was used if the data met the assumptions of normality and homogeneity of variance, otherwise Wilcoxon matched-pairs signed-rank test was used. Bland-Altman diagrams are used to assess the agreement between the measurements of two neuroradiologists. A $P < 0.05$ and corrected $P < 0.05$ (two-sided test) were considered to indicate statistical significance.

Results

The demographic and clinical characteristics of patients in JBWD group and SSWD group are shown in *Table 2*. In the JBWD group, 2 of the 11 PT patients showed too narrow contralateral sinuses that were not measured. Thus, in the JBWD group, 11 symptomatic sides and 9 contralateral sides were measured. In the SSWD group, a total of 22 symptomatic sides were measured. For the volunteer group, 36 of the 44 sides were included because 8 were too narrow to be measured (right/left, 19/17). The Bland-Altman plot shows that there is no obvious systematic deviation between the results measured by the two neuroradiologists (*Figure S1*).

Table 2 Demographic and clinical characteristics of patients

Variables	JBWD group (n=11)	SSWD group (n=22)
Age (years)	40±10	37±13
Symptomatic side		
Right	8 [73]	16 [73]
Left	3 [27]	6 [27]
BMI (kg/m ²)	24±1	23±3
Duration (months)	18±11	23±17
THI score	67±25	69±24
Clinical treatment		
Wall reconstruction	3 [27]	17 [77]
Endovascular treatment	0 [0]	2 [9]
Conservative treatment	8 [73]	3 [14]

Data are expressed as mean ± standard deviation or n [%]. JBWD, jugular bulb wall dehiscence; SSWD, sigmoid sinus wall dehiscence; BMI, body mass index; THI, tinnitus handicap inventory.

Symptomatic sinuses vs. contralateral sinuses in the JBWD group

The TS, SS, and JB hemodynamic parameters were compared between the symptomatic and contralateral sides in the JBWD group. The results are shown in *Table 3*. The area in the TS and JB on the symptomatic side was larger than that on the contralateral side ($P=0.004$, 0.034). The Q in the TS, SS, and JB on the symptomatic side was higher than that on the contralateral side, and the difference was statistically significant ($P=0.002$, 0.002 , 0.018). The V_{\max} and V_{avg} in the JB on the symptomatic side were higher than that on the contralateral side ($P=0.035$, 0.042). However, there was no significant difference in other parameters between the symptomatic and contralateral sides. *Figure 3* shows an example of a PT patient with JBWD on the right.

Statistical comparison between the SSWD group, JBWD group, and volunteer group

The area and hemodynamic quantitative values of the three groups are presented in *Table 4*. Histograms of velocities and average blood flow are represented in *Figure 4*. At the distal TS, compared with the SSWD group, the JBWD group showed a larger sinus area [45 ± 19 vs. 23 (IQR, 13 – 29) mm², corrected $P=0.004$]. Compared with the SSWD group, the JBWD group showed lower $V_{v\text{-max}}$ [67 ± 29 vs. 140 (IQR, 110 – 150) cm/s, corrected $P=0.009$], V_{\max} (30 ± 13 vs. 51 ± 17 cm/s,

corrected $P=0.021$), and V_{avg} [25 ± 10 vs. 43 (IQR, 34 – 47) cm/s, corrected $P=0.026$] at the distal TS. Compared with the volunteer group, the JBWD group showed higher $V_{v\text{-max}}$ [67 ± 29 vs. 51 (IQR, 34 – 130) cm/s, corrected $P=0.042$], V_{\max} [30 ± 13 vs. 25 (IQR, 16 – 47) cm/s, corrected $P=0.046$], and V_{avg} [25 ± 10 vs. 22 (IQR, 14 – 39) cm/s, corrected $P=0.040$] at the distal TS, and higher $V_{v\text{-max}}$ [74 ± 28 vs. 48 (IQR, 38 – 64) cm/s, corrected $P=0.007$], V_{\max} [33 ± 11 vs. 22 (IQR, 19 – 25) cm/s, corrected $P=0.001$], and V_{avg} [28 ± 10 vs. 19 (IQR, 17 – 22) cm/s, corrected $P=0.001$] at the SS. At the JB, compared with the volunteer group, the JBWD group showed higher $V_{v\text{-max}}$ [73 ± 27 vs. 53 (IQR, 42 – 72) cm/s, corrected $P=0.012$]. *Figure 5* shows a healthy volunteer with bilateral balanced venous sinuses and *Figure 6* shows a PT patient with SSWD on the right and dysplasia of the left TS.

Blood flow pattern

As for the vortex in the position of the upper curve of SS, Fisher's exact test results showed $P<0.001$ ($\chi^2=25.002$), indicating that the occurrence rates were different among the three groups. There were 2 sides (2/11, 18.2%) of vortex flow pattern in the JBWD group, 16 sides (16/22, 72.7%) in the SSWD group (18.2% vs. 72.7%, $\chi^2=8.800$, $P=0.008<0.017$), and 4 sides (4/36, 11.1%) in the volunteers (18.2% vs. 11.1%, $\chi^2=0.378$, $P=0.614>0.017$).

As for the vortex in the position of the JB, Fisher's exact test results showed $P=0.004$ ($\chi^2=10.562$), indicating that the

Table 3 The hemodynamic parameters of the bilateral TS, SS, and JB in the JBWD group

Parameters	Symptomatic side (n=9)	Asymptomatic side (n=9)	t/Z	P value
TS				
Area (mm ²)	38±16	12±4	4.426	0.004*
V _{v-max} (cm/s)	65±24	53±21	1.073	0.325
V _{max} (cm/s)	27±15	23±13	0.436	0.678
V _{avg} (cm/s)	24±13	20±12	0.553	0.6
Q (mL/s)	6.4±2.8	1.6±0.66	5.282	0.002*
SS				
Area (mm ²)	28±12	18±9.2	2.004	0.092
V _{v-max} (cm/s)	63±24	50±11	2.339	0.058
V _{max} (cm/s)	30±14	24±5.5	1.184	0.281
V _{avg} (cm/s)	26±13	21±5.2	1.077	0.323
Q (mL/s)	6.2±2.4	2.1±1.1	5.141	0.002*
JB				
Area (mm ²)	72±39	34±9.9	2.731	0.034*
V _{v-max} (cm/s)	69±29	50±19	2.082	0.083
V _{max} (cm/s)	23±11	16±5.6	2.711	0.035*
V _{avg} (cm/s)	21±11	14±5.1	2.568	0.042*
Q (mL/s)	6.4±4.1	2.4 (0.37–2.6)	–2.366	0.018 [†]

Except for the Q in the JB of the asymptomatic side expressed in median (IQR), the other parameters are expressed as mean ± standard deviation. *, significant; [†], Wilcoxon matched-pairs signed-rank test. TS, transverse sinus; SS, sigmoid sinus; JB, jugular bulb; JBWD, jugular bulb wall dehiscence; V_{v-max}, maximum voxel velocity; V_{max}, maximum velocity; V_{avg}, average velocity; Q, average blood flow rate; IQR, interquartile range.

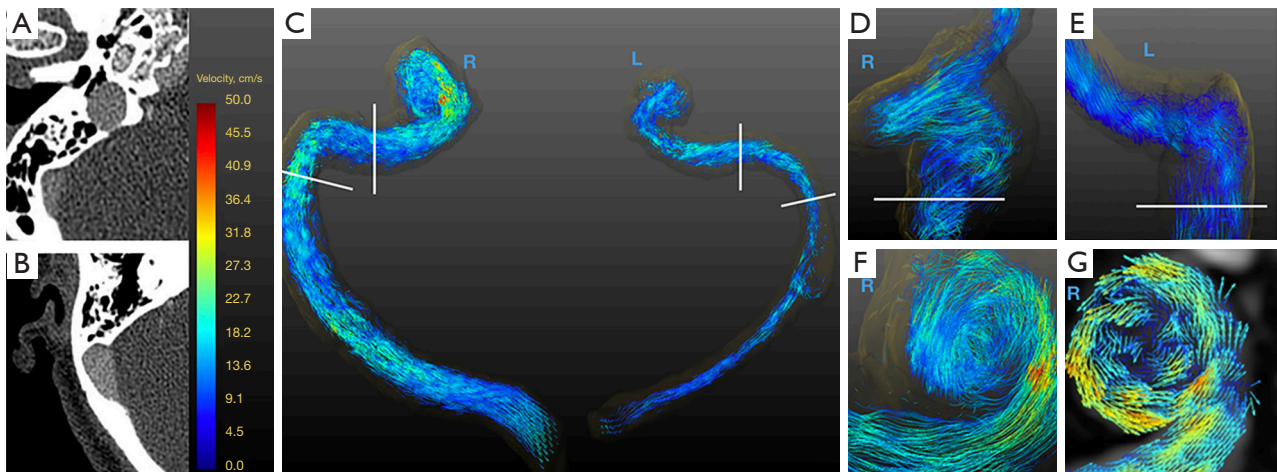


Figure 3 CTA images (A,B), streamline images (C-F), and in-plane image (G) based on 4D flow MRI of a right PT patient. CTA showed the right JBWD but no SSWD (A,B). (C-F) The streamline images of the bilateral TSs (C), SSs (D), and zoom-in images after rotation of the bilateral JBs [(E,F) are equivalent to the front view; (G) is equivalent to the top view]. The vortex flow pattern is seen at the right JB (G). The white horizontal lines represent the sites of hemodynamic measurement (C-E). CTA, computed tomography angiography; 4D, four-dimensional; MRI, magnetic resonance imaging; PT, pulsatile tinnitus; JBWD, jugular bulb wall dehiscence; SSWD, sigmoid sinus wall dehiscence; TS, transverse sinus; SS, sigmoid sinus; JB, jugular bulb.

Table 4 The comparison of the measured values among the three groups

Parameters	Area (mm ²)	V _{v-max} (cm/s)	V _{max} (cm/s)	V _{avg} (cm/s)	Q (mL/s)
TS					
JBWD group	45±19	67±29	30±13	25±10	7.3±3.7
SSWD group	23 [13, 29]	140 [110, 150]	51±17	43 [34, 47]	5.5±2.4
Volunteer group	36±15	51 [34, 130]	25 [16, 47]	22 [14, 39]	4.6±2.3
P ₀ (H)	0.002 (12.572)	<0.001 (51.951)	<0.001 (46.384)	<0.001 (45.991)	0.053 (5.868)
P ₁	0.004	0.009	0.021	0.026	–
P ₂	0.533	0.042	0.046	0.040	–
SS					
JBWD group	29±12	74±28	33±11	28±10	6.4±2.4
SSWD group	35 [31, 38]	55 [48, 78]	24 [21, 28]	21 [18, 25]	5.4±1.4
Volunteer group	32±14	48 [38, 64]	22 [19, 25]	19 [17, 22]	4.6±2.4
P ₀ (H)	0.538 (1.385)	<0.001 (18.924)	0.003 (13.638)	0.003 (13.920)	0.140 (4.404)
P ₁	–	>0.99	0.448	0.368	–
P ₂	–	0.007	0.001	0.001	–
JB					
JBWD group	69±34	73±27	23±10	19±4.2	7.8±5.5
SSWD group	55 [42, 73]	71 [52, 86]	22±4.5	21±9.9	5.3±2.1
Volunteer group	60±18	53 [42, 72]	20 [18, 24]	18 [15, 19]	4.9±2.1
P ₀ (H)	0.427 (1.702)	<0.001 (16.039)	0.129 (4.101)	0.197 (3.246)	0.195 (3.269)
P ₁	–	>0.99	–	–	–
P ₂	–	0.012	–	–	–

Continuous variables with normal distribution were expressed as mean ± standard deviation and continuous variables with non-normal distribution were expressed as median [IQR]. P₀: the significance of one-way ANOVA or Kruskal-Wallis H test among the three groups. If P₀>0.05, multiple comparisons are not performed. P₁: JBWD group vs. SSWD group (significance values have been adjusted by the Bonferroni correction for multiple tests). P₂: JBWD group vs. volunteer group (significance values have been adjusted by the Bonferroni correction for multiple tests). TS, transverse sinus; SS, sigmoid sinus; JB, jugular bulb; JBWD, jugular bulb wall dehiscence; SSWD, sigmoid sinus wall dehiscence; V_{v-max}, voxel maximum velocity; V_{max}, maximum velocity; V_{avg}, average velocity; Q, average blood flow; ANOVA, analysis of variance; IQR, interquartile range.

occurrence rates were different among the three groups. There were 10 sides (10/11, 90.9%) of vortex flow pattern in the JBWD group, 9 sides (9/22, 40.9%) in the SSWD group (90.9% vs. 40.9%, $\chi^2=10.125$, P=0.002<0.017), and 13 sides (13/36, 36.1%) in the volunteers (90.9% vs. 36.1%, $\chi^2=7.506$, P=0.009<0.017). *Videos 1,2* show the vortex of the JBWD group and the SSWD group patients, respectively.

Discussion

In this study, 4D flow MRI was used to describe the

hemodynamics of TS, SS, and JB in PT patients and volunteers, and moreover, compare the hemodynamics of the JBWD group and the SSWD group. The JBWD group showed higher values of V_{v-max}, V_{max}, and V_{avg} in the TS and SS than the volunteer group, as well as a higher frequency of vortex formation at the JB. These parameters, namely V_{v-max}, V_{max}, V_{avg}, TS cross-sectional area, and vortex, can serve as biomarkers to differentiate the JBWD group from the SSWD group.

Bone wall dehiscence is a key cause of PT, which is well evidenced by previous surgical repair (13,29,30). It has also

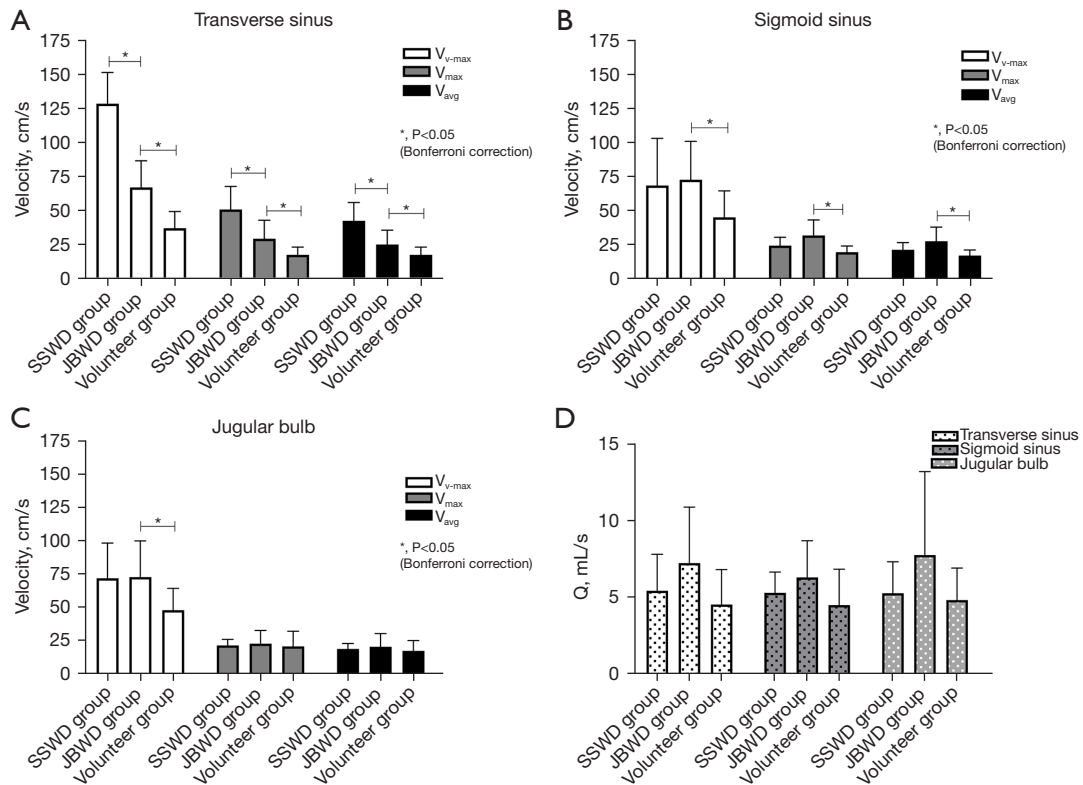


Figure 4 Blood flow parameters in different vascular segments in the JBWD group, the SSWD group, and the volunteer group. (A) The V_{v-max} , V_{max} , and V_{avg} values of the TS in the JBWD group, the SSWD group, and the volunteer group. (B) The same parameters as in (A) for the SS. (C) The same parameters as in (A) for the JB. (D) The Q values of the JBWD group, the SSWD group, and the volunteer group in the TS, the SS, and the JB. The asterisk (*) denotes a statistically significant difference in the P value after Bonferroni correction between the two groups. V_{v-max} , maximum voxel velocity; V_{max} , maximum velocity; V_{avg} , average velocity; SSWD, sigmoid sinus wall dehiscence; JBWD, jugular bulb wall dehiscence; Q, average blood flow rate; TS, transverse sinus; SS, sigmoid sinus; JB, jugular bulb.

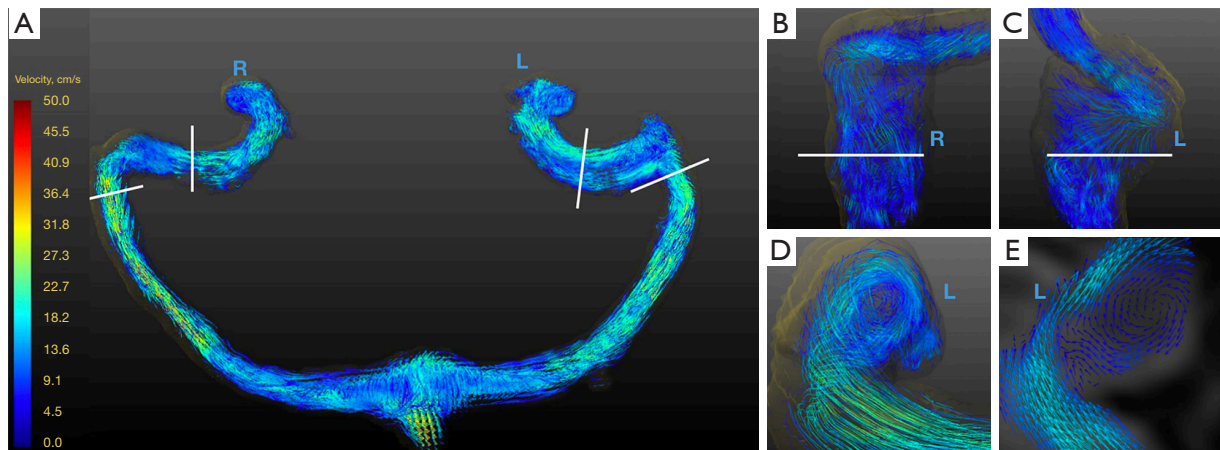


Figure 5 Streamline images of a healthy volunteer based on 4D flow MRI. (A-D) Images of bilateral TSs (A), SSs (A), and zoom-in images after rotation of bilateral JBWs [(B,C) are equivalent to the front view; (D) is equivalent to the top view]. The vortex flow pattern is seen at the right JB (D,E). The white horizontal lines represent the sites of hemodynamic measurement (A-C). R, right; L, left; 4D, four-dimensional; MRI, magnetic resonance imaging; TS, transverse sinus; SS, sigmoid sinus; JB, jugular bulb.

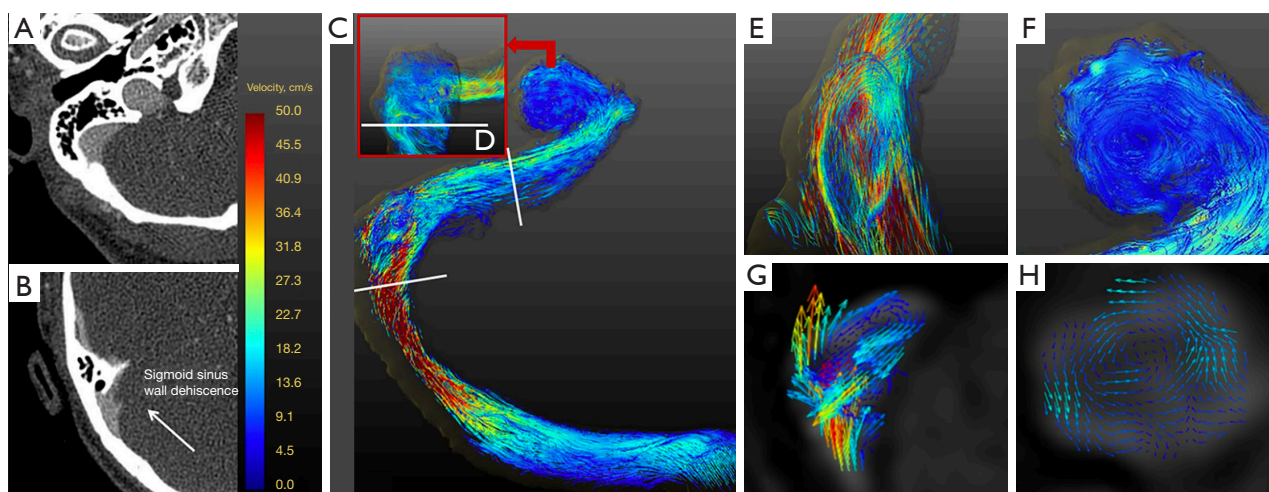


Figure 6 CTA images (A,B), streamline images (C-F), and in-plane images (G,H) based on 4D flow MRI of a right PT patient. CTA showed the right SSWD but no JBWD (A,B). (C-F) The streamline images of the TS (C), SS (C), and zoom-in images after rotation of the JB [(D) is equivalent to the front view]. The vortex flow pattern is seen at the upper curve of the SS (E,G) and the right JB (F,H). The white horizontal lines represent the sites of hemodynamic measurement (C,D). CTA, computed tomography angiography; 4D, four-dimensional; MRI, magnetic resonance imaging; PT, pulsatile tinnitus; SSWD, sigmoid sinus wall dehiscence; JBWD, jugular bulb wall dehiscence; TS, transverse sinus; SS, sigmoid sinus; JB, jugular bulb.



Video 1 CTA and 4D flow MRI dynamic images of a patient with right PT. The CTA reveals that the patient has only JBWD without SSWD. The 4D flow MRI demonstrates the vortex flow at the JB. CTA, computed tomography angiography; 4D, four-dimensional; MRI, magnetic resonance imaging; PT, pulsatile tinnitus; JBWD, jugular bulb wall dehiscence; SSWD, sigmoid sinus wall dehiscence; JB, jugular bulb.



Video 2 CTA and 4D flow MRI dynamic images of a patient with right PT. The CT angiography reveals that the patient has only SSWD without JBWD. The 4D flow MRI demonstrates the vortex flow at the upper curve of the SS and JB. CTA, computed tomography angiography; 4D, four-dimensional; MRI, magnetic resonance imaging; PT, pulsatile tinnitus; SSWD, sigmoid sinus wall dehiscence; JBWD, jugular bulb wall dehiscence; SS, sigmoid sinus; JB, jugular bulb.

been reported that cortical plate dehiscence significantly contributed to noise sensation (12). CT is commonly used to assess the integrity of the bone wall around the venous sinuses. However, not all bone wall defects around the

venous sinus could lead to PT symptoms (31,32). Our results indicate that 12.7% of PT patients present with both JBWD and SSWD, which complicates the identification of the responsible symptomatic bone wall dehiscence.

Thus, after excluding other possible causes, PT patients who had been previously diagnosed with either JBWD or SSWD were included in this study to ensure the accuracy of identifying PT etiology to the greatest extent.

In previous studies, PT caused by SSWD was usually concerned with the hemodynamics and morphology of the upstream TS (14,15), whereas PT caused by JBWD was usually concerned with the hemodynamics at the JB (17). This study innovatively assessed the blood flow of three successive segments in three populations, which more completely revealed the correlation between intracranial venous sinus blood flow and different PT types. Meanwhile, previous researchers mainly adopted voxel maximum blood flow velocity based on 4D flow MRI (14), and this study also focused on the maximal velocity of the plane.

The PT patients in the JBWD group had lower velocity in the TS than the SSWD group and higher than the healthy volunteer group, which could be used as an important hemodynamic biomarker to differentiate the three groups. This study also found that the SSWD group had a smaller area at the proximal end of the TS, which narrowed and accelerated the blood flow. This finding was consistent with most previous reports (14,15,19). The JBWD group had less narrowing at the proximal end of the TS than the SSWD group, resulting in less velocity increase. Therefore, high-speed blood flow was the cause of PT originating from the SSWD, not from the JBWD group. Although the JBWD group had faster blood flow velocity than the healthy volunteers, the increased blood flow velocity was not sufficient to induce abnormal changes in the SS bone wall.

In prior work, the diameter or cross-sectional area of the TS, as revealed by angiography, was frequently utilized to infer blood flow (1,33,34). In the present work, 4D flow MRI was used to describe the blood flow directly and accurately. In the JBWD group, the blood flow of the symptomatic side was higher than that of the contralateral side in all three measurement planes. This finding was consistent with previous studies that reported PT induced by SSWD (14). This indicates that the occurrence of PT requires a large blood flow rate, suggesting that PT is more likely to occur on the dominant side. The histogram indicated that the blood flow rate of the JBWD group was higher than that of the SSWD group. A possible explanation for the mismatch in blood flow rate and blood flow velocity at the TS is the larger cross-area of the TS in the JBWD group. However, the difference did not reach statistical significance, which might be explained by the small number of patients in our study.

Previous studies have established TS stenosis as a critical factor for PT development, which could increase the trans-stenotic pressure gradient, velocity, and force (14,18,35). These factors lead to the continuous erosion of the SS wall by the blood flow, resulting in its thinning and deformation. In this study, the JBWD group was found to have a larger cross-sectional area of the TS at the proximal end than the SSWD group, which caused more blood flow to diffuse outward and thus reduced the blood flow velocity and increased the blood flow rate. This finding supported that the accelerated blood flow velocity was the main cause of the SSWD from a different perspective. Therefore, the cross-sectional area of the TS at the proximal end could be used as one of the criteria to differentiate the SSWD group, which was responsible for the mismatch between the blood flow velocity and rate in both groups.

The vortex pattern was thought to be associated with PT (14,17,35-37). This study showed that the vortex in the SSWD group tends to occur in the SS, and the vortex in the JBWD group tends to occur in the JB. These findings are consistent with previous studies that demonstrated that upstream fast flow could generate downstream vortices and that the occurrence of vortices at the JB may depend on their elevated position or irregular shape (17,35,36). However, the exact mechanism underlying the development of PT by vortex flow patterns remains elusive. It may be associated with the activation of the cochlear inner hair cells due to the noise energy produced by vortices or the mechanical damage of vortices to the adjacent bone wall resulting in its thinning or disappearance.

These results indicate that the hemodynamics of the two types of PT differ, suggesting that the etiology of the two types of PT also varies, and thus the treatment methods based on the etiology may differ as well. Previous studies have demonstrated that endovascular treatment is highly effective and safe for PT patients who often present with TS stenosis and SSWD (18,37,38). Endovascular stenting can not only alleviate symptoms but also ameliorate the abnormal condition of the SS bone wall (18,39). However, according to the results of this study, the blood flow velocity of the PT patients in the JBWD group is lower than that of the SSWD group, and reducing blood flow velocity may not be effective for them. This may also explain why few studies have been reported to use endovascular stenting for PT patients with JBWD (40). In this study, it was found that 12.7% of venous PT patients had both SSWD and JBWD, which may pose a challenge in determining the etiology. In this situation, the hemodynamic results may be

helpful for further identifying the source of the sound, and thus selecting the suitable treatment strategy.

This study has some limitations. First, the JBWD group had a small sample size recruited from a single institution. This was because JBWD had a lower incidence than SSWD (7); our strict inclusion criteria only allowed JBWD patients, not those with both JBWD and SSWD. Second, we enrolled only female patients in the three groups, as all the JBWD patients who met the criteria were female. This was mainly due to the high prevalence of female PT patients (41) which prevented us from assessing possible sex-related differences in hemodynamics between men and women. Third, although we tried to avoid measuring at the locations where vortices were most prominent, there might still have been flow quantification errors caused by non-laminar flow and acceleration at the upper curve of the SS and JB. Fourth, not all JBWD patients obtained surgical confirmation, mainly because of the complexity of the surgery and the lack of knowledge about the preoperative features of this type of PT. Compared with PT caused by SSWD, PT caused by JBWD has received less attention and investigation in terms of imaging and hemodynamic characteristics, which poses challenges and uncertainties for the diagnosis and treatment of this type of PT. Therefore, fewer patients opted for surgical treatment. Fifth, no additional hemodynamic models, such as computational fluid dynamics and ultrasound, were used to verify the data in this study. The conclusions need to be further verified in the future.

Conclusions

In summary, this study utilized 4D flow MRI to measure and visualize intracranial blood flow *in vivo* in PT patients with JBWD and contrasted them with the SSWD group. Differences in cerebral sinus hemodynamics and treatment options between the JBWD and SSWD groups indicate the need to distinguish the two types of PT in clinical work and research. PT patients with both JBWD and SSWD in clinical settings can undergo the 4D flow MRI examination to help identify the main source of noise. The indicators that can differentiate include V_{v-max} , V_{max} , V_{avg} , vortex, and TS cross-sectional area.

Acknowledgments

Funding: This work was supported by the National Natural Science Foundation of China (No. 61931013 to Z.C.W.,

No. 82171886 to P.F.Z., No. 82202098 to H.Y.D., and No. 62171297 to H.L.), the Natural Science Foundation of Beijing Municipality (No. 7222301 to P.F.Z.), the Beijing Scholars Program (No. [2015] 160 to Z.C.W.), and the Beijing key Clinical Discipline Funding (No. 2021-135 to Z.C.W.).

Footnote

Reporting Checklist: The authors have completed the STROBE reporting checklist. Available at <https://qims.amegroups.com/article/view/10.21037/qims-23-781/rc>

Conflicts of Interest: All authors have completed the ICMJE uniform disclosure form (available at <https://qims.amegroups.com/article/view/10.21037/qims-23-781/coif>). The authors have no conflicts of interest to declare.

Ethical Statement: The authors are accountable for all aspects of the work in ensuring that questions related to the accuracy or integrity of any part of the work are appropriately investigated and resolved. The study was conducted in accordance with the Declaration of Helsinki (as revised in 2013). The study was approved by the Ethics Committee of Beijing Friendship Hospital Affiliated to Capital Medical University (Nos. 2020-P2-202-02, 2023-P2-095-01), and all patients provided written informed consent.

Open Access Statement: This is an Open Access article distributed in accordance with the Creative Commons Attribution-NonCommercial-NoDerivs 4.0 International License (CC BY-NC-ND 4.0), which permits the non-commercial replication and distribution of the article with the strict proviso that no changes or edits are made and the original work is properly cited (including links to both the formal publication through the relevant DOI and the license). See: <https://creativecommons.org/licenses/by-nc-nd/4.0/>.

References

1. Zhao P, Lv H, Dong C, Niu Y, Xian J, Wang Z. CT evaluation of sigmoid plate dehiscence causing pulsatile tinnitus. *Eur Radiol* 2016;26:9-14.
2. Lockwood AH, Salvi RJ, Burkard RF. Tinnitus. *N Engl J Med* 2002;347:904-10.
3. Zheng W, Peng Z, Pengfei Z, Jing L, Heyu D, Hongxia Y, Yawen L, Zhengyu Z, Shusheng G, Zhenghan Y,

- Han L, Zhenchang W. Long-term reactions to pulsatile tinnitus are marked by weakened short-range functional connectivity within a brain network in the right temporal lobe. *J Magn Reson Imaging* 2019;49:1629-37.
4. Erlandsson SI, Hallberg LR. Prediction of quality of life in patients with tinnitus. *Br J Audiol* 2000;34:11-20.
 5. Tao AJ, Parikh NS, Patsalides A. The role of noninvasive imaging in the diagnostic workup for pulsatile tinnitus. *Neuroradiol J* 2022;35:220-5.
 6. Mattox DE, Hudgins P. Algorithm for evaluation of pulsatile tinnitus. *Acta Otolaryngol* 2008;128:427-31.
 7. Dong C, Zhao PF, Yang JG, Liu ZH, Wang ZC. Incidence of vascular anomalies and variants associated with unilateral venous pulsatile tinnitus in 242 patients based on dual-phase contrast-enhanced computed tomography. *Chin Med J (Engl)* 2015;128:581-5.
 8. Liyanage SH, Singh A, Savundra P, Kalan A. Pulsatile tinnitus. *J Laryngol Otol* 2006;120:93-7.
 9. Miller TR, Serulle Y, Gandhi D. Arterial Abnormalities Leading to Tinnitus. *Neuroimaging Clin N Am* 2016;26:227-36.
 10. Lyu AR, Park SJ, Kim D, Lee HY, Park YH. Radiologic features of vascular pulsatile tinnitus - suggestion of optimal diagnostic image workup modalities. *Acta Otolaryngol* 2018;138:128-34.
 11. Narsinh KH, Hui F, Saloner D, Tu-Chan A, Sharon J, Rauschecker AM, Safoora F, Shah V, Meisel K, Amans MR. Diagnostic Approach to Pulsatile Tinnitus: A Narrative Review. *JAMA Otolaryngol Head Neck Surg* 2022;148:476-83.
 12. Tian S, Wang L, Yang J, Mao R, Liu Z, Fan Y. Sigmoid sinus cortical plate dehiscence induces pulsatile tinnitus through amplifying sigmoid sinus venous sound. *J Biomech* 2017;52:68-73.
 13. Yeo WX, Xu SH, Tan TY, Low YM, Yuen HW. Surgical management of pulsatile tinnitus secondary to jugular bulb or sigmoid sinus diverticulum with review of literature. *Am J Otolaryngol* 2018;39:247-52.
 14. Li Y, Chen H, He L, Cao X, Wang X, Chen S, Li R, Yuan C. Hemodynamic assessments of venous pulsatile tinnitus using 4D-flow MRI. *Neurology* 2018;91:e586-93.
 15. Li X, Qiu X, Ding H, Lv H, Zhao P, Yang Z, Gong S, Wang Z. Effects of different morphologic abnormalities on hemodynamics in patients with venous pulsatile tinnitus: A four-dimensional flow magnetic resonance imaging study. *J Magn Reson Imaging* 2021;53:1744-51.
 16. Mu Z, Qiu X, Zhao D, Li X, Fu M, Liu Y, Gao B, Zhao P, Wang Z. Hemodynamic study on the different therapeutic effects of SSWD resurfacing surgery on patients with pulsatile tinnitus. *Comput Methods Programs Biomed* 2020;190:105373.
 17. Kao E, Kefayati S, Amans MR, Faraji F, Ballweber M, Halbach V, Saloner D. Flow patterns in the jugular veins of pulsatile tinnitus patients. *J Biomech* 2017;52:61-7.
 18. Han Y, Xia J, Jin L, Qiao A, Su T, Li Z, Xiong J, Wang H, Zhang Z. Computational fluid dynamics study of the effect of transverse sinus stenosis on the blood flow pattern in the ipsilateral superior curve of the sigmoid sinus. *Eur Radiol* 2021;31:6286-94.
 19. Dai C, Zhao P, Ding H, Lv H, Qiu X, Li X, Xu N, Meng X, Wang G, Xie J, Yang Z, Gong S, Wang Z. CT evaluation of unilateral pulsatile tinnitus with jugular bulb wall dehiscence. *Eur Radiol* 2023;33:4464-71.
 20. Manara R, Mardari R, Ermani M, Severino MS, Santelli L, Carollo C. Transverse dural sinuses: incidence of anatomical variants and flow artefacts with 2D time-of-flight MR venography at 1 Tesla. *Radiol Med* 2010;115:326-38.
 21. Stolz E, Kaps M, Kern A, Babacan SS, Dorndorf W. Transcranial color-coded duplex sonography of intracranial veins and sinuses in adults. Reference data from 130 volunteers. *Stroke* 1999;30:1070-5.
 22. Manninen AL, Isokangas JM, Karttunen A, Siniluoto T, Nieminen MT. A comparison of radiation exposure between diagnostic CTA and DSA examinations of cerebral and cervicocerebral vessels. *AJNR Am J Neuroradiol* 2012;33:2038-42.
 23. Pereira VM, Delattre B, Brina O, Bouillot P, Vargas MI. 4D Flow MRI in Neuroradiology: Techniques and Applications. *Top Magn Reson Imaging* 2016;25:81-7.
 24. Zhang M, Peng F, Li Y, He L, Liu A, Li R. Associations between morphology and hemodynamics of intracranial aneurysms based on 4D flow and black-blood magnetic resonance imaging. *Quant Imaging Med Surg* 2021;11:597-607.
 25. Schrauben EM, Kohn S, Macdonald J, Johnson KM, Kliewer M, Frost S, Fleming JO, Wieben O, Field A. Four-dimensional flow magnetic resonance imaging and ultrasound assessment of cerebrospinal venous flow in multiple sclerosis patients and controls. *J Cereb Blood Flow Metab* 2017;37:1483-93.
 26. Rivera-Rivera LA, Schubert T, Turski P, Johnson KM, Berman SE, Rowley HA, Carlsson CM, Johnson SC, Wieben O. Changes in intracranial venous blood flow and pulsatility in Alzheimer's disease: A 4D flow MRI study. *J Cereb Blood Flow Metab* 2017;37:2149-58.

27. Fu M, Peng F, Zhang M, Chen S, Niu H, He X, Xu B, Liu A, Li R. Aneurysmal wall enhancement and hemodynamics: pixel-level correlation between spatial distribution. *Quant Imaging Med Surg* 2022;12:3692-704.
28. Battal B, Zamora C. Editorial Comment: Estimation of venous sinus pressure drop in patients with idiopathic intracranial hypertension using 4D-flow MRI. *Eur Radiol* 2023;33:2574-5.
29. Liu GS, Boursiquot BC, Blevins NH, Vaisbuch Y. Systematic Review of Temporal Bone-Resurfacing Techniques for Pulsatile Tinnitus Associated with Vascular Wall Anomalies. *Otolaryngol Head Neck Surg* 2019;160:749-61.
30. DeHart AN, Shaia WT, Coelho DH. Hydroxyapatite cement resurfacing the dehiscent jugular bulb: Novel treatment for pulsatile tinnitus. *Laryngoscope* 2018;128:1186-90.
31. Sayit AT, Gunbey HP, Fethallah B, Gunbey E, Karabulut E. Radiological and audiometric evaluation of high jugular bulb and dehiscent high jugular bulb. *J Laryngol Otol* 2016;130:1059-63.
32. Atmaca S, Elmali M, Kucuk H. High and dehiscent jugular bulb: clear and present danger during middle ear surgery. *Surg Radiol Anat* 2014;36:369-74.
33. Carvalho GB, Matas SL, Idagawa MH, Tibana LA, de Carvalho RS, Silva ML, Cogo-Moreira H, Jackowski AP, Abdala N. A new index for the assessment of transverse sinus stenosis for diagnosing idiopathic intracranial hypertension. *J Neurointerv Surg* 2017;9:173-7.
34. Eisenman DJ, Raghavan P, Hertzano R, Morales R. Evaluation and treatment of pulsatile tinnitus associated with sigmoid sinus wall anomalies. *Laryngoscope* 2018;128 Suppl 2:S1-S13.
35. Ding H, Zhao P, Lv H, Li X, Qiu X, Zeng R, Wang G, Yang Z, Gong S, Jin L, Wang Z. Correlation Between Trans-Stenotic Blood Flow Velocity Differences and the Cerebral Venous Pressure Gradient in Transverse Sinus Stenosis: A Prospective 4-Dimensional Flow Magnetic Resonance Imaging Study. *Neurosurgery* 2021;89:549-56.
36. Acevedo-Bolton G, Amans MR, Kefayati S, Halbach V, Saloner D. Four dimensional magnetic resonance velocimetry for complex flow in the jugular vein. *Quant Imaging Med Surg* 2015;5:635-7.
37. Pereira VM, Cancelliere NM, Najafi M, MacDonald D, Natarajan T, Radovanovic I, Krings T, Rutka J, Nicholson P, Steinman DA. Torrents of torment: turbulence as a mechanism of pulsatile tinnitus secondary to venous stenosis revealed by high-fidelity computational fluid dynamics. *J Neurointerv Surg* 2021;13:732-7.
38. Boddu S, Dinkin M, Suurna M, Hannsge K, Bui X, Patsalides A. Resolution of Pulsatile Tinnitus after Venous Sinus Stenting in Patients with Idiopathic Intracranial Hypertension. *PLoS One* 2016;11:e0164466.
39. Qiu XY, Zhao PF, Ding HY, Li XS, Lv H, Yang ZH, Gong SS, Jin L, Wang ZC. Bone remodeling in sigmoid sinus diverticulum after stenting for transverse sinus stenosis in pulsatile tinnitus: A case report. *World J Clin Cases* 2021;9:2320-5.
40. Essibayi MA, Oushy SH, Lanzino G, Brinjikji W. Venous Causes of Pulsatile Tinnitus: Clinical Presentation, Clinical and Radiographic Evaluation, Pathogenesis, and Endovascular Treatments: A Literature Review. *Neurosurgery* 2021;89:760-8.
41. Lynch P, Mitton T, Killeen DE, Kutz JW, Newcomer M. Diagnosing Pulsatile Tinnitus: A Review of 251 Patients. *Otol Neurotol* 2022;43:128-36.

Cite this article as: Dai C, Zhao P, Wang G, Ding H, Lv H, Qiu X, Tang R, Xu N, Huang Y, He K, Yang Z, Gong S, Wang Z. Hemodynamic assessments of unilateral pulsatile tinnitus with jugular bulb wall dehiscence using 4D flow magnetic resonance imaging. *Quant Imaging Med Surg* 2024;14(1):684-697. doi: 10.21037/qims-23-781

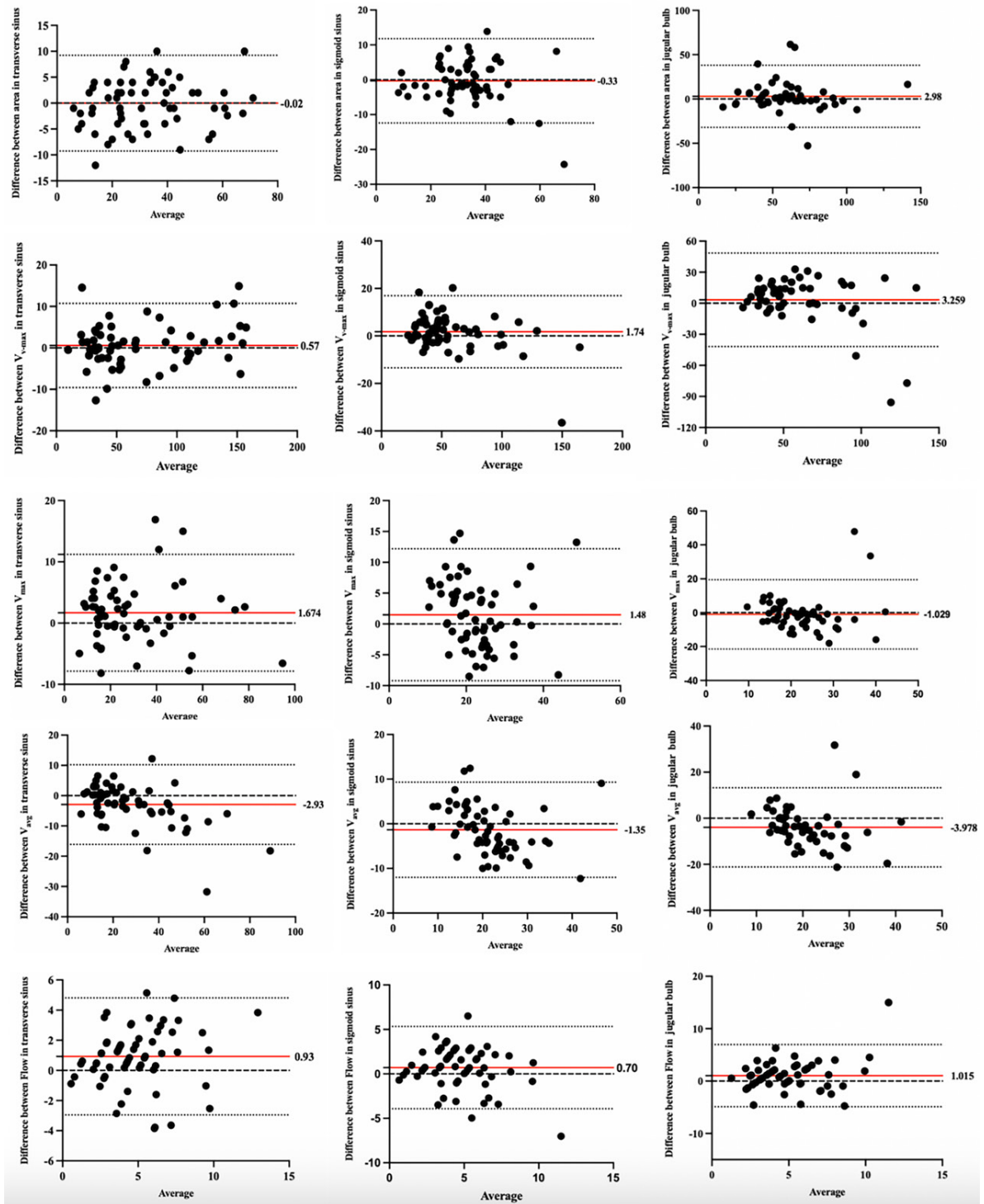


Figure S1 Bland-Altman plots are used to show the agreement between the measurements of two neuroradiologists for the area, V_{v-max} , V_{max} , V_{avg} and Q . Bland-Altman plots show no substantial systematic bias between the two neuroradiologists. V_{v-max} maximum voxel velocity; V_{max} maximum velocity; V_{avg} average velocity; Q , average blood flow rate.